

Neural Network-Assisted Reconstruction of Full Polarimetric SAR Information

Thanh-Hai Le, Ian McLoughlin *Senior Member, IEEE*, Ken Yoong Lee and Timo Bretschneider

Abstract—This paper describes a novel approach to the reconstruction of synthetic aperture radar (SAR) fully polarimetric data from compact polarimetry (CP) $\pi/4$ mode. A method is developed which utilises a multi-layer perceptron (MLP) based neural network, to perform reconstruction of scenes with various ground-cover types. In particular, the approach shows potential for the reconstruction of full polarimetry for built-up areas as a complement to existing techniques which are more suitable for natural land cover areas.

Performance assessment is presented, using both L-band and C-band data, involving comparison with existing techniques using mean-squared and mean-squared-log measures.

Index Terms - polarimetric synthetic aperture radar, compact polarimetry, multi-layer perceptron, neural network

I. INTRODUCTION

Compact polarimetry, in which each element of an image is described using a subset of the full data, can be an attractive design proposition for many polarimetric synthetic aperture radar (POLSAR) systems due to the reduced storage requirements, reduced download data rate, and reduced radar power consumption. This is particularly so for space-borne systems, and in other deployments where significant limits on weight or power consumption have been imposed.

Allied to these advantages is the consequent ability for such systems to increase azimuth sampling frequency, increase swath width or alternatively reduced the bandwidth demands for satellite data downlink over full polarimetry (FP) [1].

However, the trade-off for these gains is the reduction in the amount of information conveyed with CP, as well as in a reduced ability to synthesize target responses or polarimetric signatures, for any transmitted and received radar polarisation [2]. Furthermore some analysis and processing systems assume and require FP input data, leading to the need for a process capable of reconstructing this FP information from the CP data: ideally a process which is both accurate and computationally simple.

In a pioneering study of this area, Souyris et al. [3] introduced compact polarimetry and coined the term ' $\pi/4$ mode', where the target vector is defined as shown in Eqn. (1):

*Manuscript received 29 October 2009.

Thanh-Hai Le and Ian McLoughlin are with the School of Computer Engineering, Block N4, Nanyang Avenue, Nanyang Technological University, Singapore 639798, e-mail: {teth0011, mcloughlin}@ntu.edu.sg

Ken Yoong Lee and Timo Bretschneider are with EADS Innovation Works Singapore, 41 Science Park Road #01-30 The Gemini, Science Park II, Singapore 117610, e-mail: {ken-yoong.lee, timo.bretschneider}@eads.net

$$t_{CP} = [s_{HH} + s_{HV} \quad s_{HV} + s_{VV}]^T \quad (1)$$

instead of the full polarimetric (FP) vector in Eqn. (2):

$$t_{FP} = [s_{HH} \quad \sqrt{2}s_{HV} \quad s_{VV}]^T. \quad (2)$$

The notation s_{HH} denotes the scattering element for horizontal-horizontal polarization. The corresponding covariance matrices for both CP and FP modes are \mathbf{J} and \mathbf{C} respectively:

$$\mathbf{J} = \begin{bmatrix} |s_{HH}|^2 + |s_{HV}|^2 & s_{HH}s_{VV}^* + |s_{HV}|^2 \\ s_{HH}^*s_{VV} + |s_{HV}|^2 & |s_{HV}|^2 + |s_{VV}|^2 \end{bmatrix} + \begin{bmatrix} 2 * \Re(s_{HH}s_{HV}^*) & s_{HH}s_{HV}^* + s_{HV}s_{VV}^* \\ s_{HV}s_{HH}^* + s_{VV}s_{HV}^* & 2 * \Re(s_{VV}s_{HV}^*) \end{bmatrix}, \quad (3)$$

$$\mathbf{C} = \begin{bmatrix} |s_{HH}|^2 & \sqrt{2}s_{HH}s_{HV}^* & s_{HH}s_{VV}^* \\ \sqrt{2}s_{HV}s_{HH}^* & 2|s_{HV}|^2 & \sqrt{2}s_{HV}s_{VV}^* \\ s_{VV}s_{HH}^* & \sqrt{2}s_{VV}s_{HV}^* & |s_{VV}|^2 \end{bmatrix}. \quad (4)$$

Comparing Eqns. (3) and (4), it is clear that the measurable data in CP reduces from nine to four unique data elements per pixel, leading to the potential for significant savings in storage requirements and transmission bandwidth. However, where only CP data is available but FP data is required, an FP matrix needs to be reconstructed from the reduced CP information set. From only four known measurable data elements in CP, nine unknown data elements in the FP matrix need to be obtained in some way.

Fortunately, this under-determined estimation process can be constrained in some cases by applying a symmetry assumption, where the following condition holds:

$$s_{HH}s_{HV}^* = s_{HV}s_{HH}^* = s_{HV}s_{VV}^* = s_{VV}s_{HV}^* = 0 \quad (5)$$

This assumption has been shown to be applicable for natural surfaces [4], and allows matrix \mathbf{J} in Eqn. (3) to be simplified as follows:

$$\mathbf{J} = \begin{bmatrix} |s_{HH}|^2 + |s_{HV}|^2 & s_{HH}s_{VV}^* + |s_{HV}|^2 \\ s_{HH}^*s_{VV} + |s_{HV}|^2 & |s_{HV}|^2 + |s_{VV}|^2 \end{bmatrix} \quad (6)$$

Furthermore, the matrix \mathbf{C} in Eqn. (4) now becomes:

$$\mathbf{C} = \begin{bmatrix} |s_{HH}|^2 & 0 & s_{HH}s_{VV}^* \\ 0 & 2|s_{HV}|^2 & 0 \\ s_{VV}s_{HH}^* & 0 & |s_{VV}|^2 \end{bmatrix} \quad (7)$$

or

$$\mathbf{C} = \begin{bmatrix} j_{11} - |s_{HV}|^2 & 0 & j_{12} - |s_{HV}|^2 \\ 0 & 2|s_{HV}|^2 & 0 \\ j_{12}^* - |s_{HV}|^2 & 0 & j_{22} - |s_{HV}|^2 \end{bmatrix} \quad (8)$$

where $j_{n,m}$ are elements of the matrix \mathbf{J} .

It is worthwhile noting that Eqn. (8) describes a much more straightforward approach for reconstructing the FP data, i.e. five elements need to be obtained from four known data elements. Thus, given the symmetry assumption, only the extra unknown element $|s_{HV}|^2$ needs to be estimated to reconstruct FP information from CP measured data.

In order to estimate $|s_{HV}|^2$, Souyris et al. [3] proposed a 'pseudo-deterministic' relationship between h-v correlation coefficient $|\rho_{h-v}|$ and the average cross polarization ratio $\frac{|s_{HV}|^2}{(|s_{HH}|^2 + |s_{VV}|^2)}$. It is observed that, for a fully polarized back-scattered wave, $|s_{HV}|^2 = 0$ and $|\rho_{h-v}|^2 = 1$, while for a fully depolarized wave $|\rho_{h-v}|^2 \approx 0$ and $|s_{HH}|^2 + |s_{VV}|^2 \approx 2|s_{HV}|^2$. Thus a linear extrapolated relationship is developed which is given as

$$\frac{|s_{HV}|^2}{(|s_{HH}|^2 + |s_{VV}|^2)} = \frac{(1 - |\rho_{h-v}|)}{4}.$$

Based upon this model, Souyris et. al. undertook a numerical estimation approach to determine $|s_{HV}|^2$, and thus proceed to reconstruct full polarimetry information. This was then followed by an evaluation of the system based upon agricultural land classification performance. More recently, Nord et al. [5] demonstrated that the actual relationship is, in fact, significantly non-linear (for their utilised dataset), and thus proposed a refined estimation procedure, obtaining better results.

It is significant that Nord et al. maintained the same symmetry assumption in order to simplify the FP reconstruction. This means that the improved technique, like the original, is best suited to natural surface reflection. The authors of both papers clearly identify this proviso in their work.

In this paper, we extend the CP to FP reconstruction of $\pi/4$ mode data without making any symmetry or linearity assumption, by building an MLP-based reconstructor. We evaluate the system against the Souyris et al. benchmark both for agricultural land cover, but also extend the evaluation to built up areas where we expect the symmetry assumption to be violated, and thus the existing benchmarks to perform relatively poorly.

II. USE OF MLP FOR FULL POLARIMETRY RECONSTRUCTION

In this paper, the learning capability of a MLP NN is employed to build a system capable of estimating FP information from CP data, and is evaluated by comparing the reconstructed FP data to full data.

Evidently, the evaluation requires an actual FP data set for comparison. Thus CP input data is derived first from this FP data set. It is important to note that, since we do not make any symmetry assumption, we can not simulate CP data using Eqn.

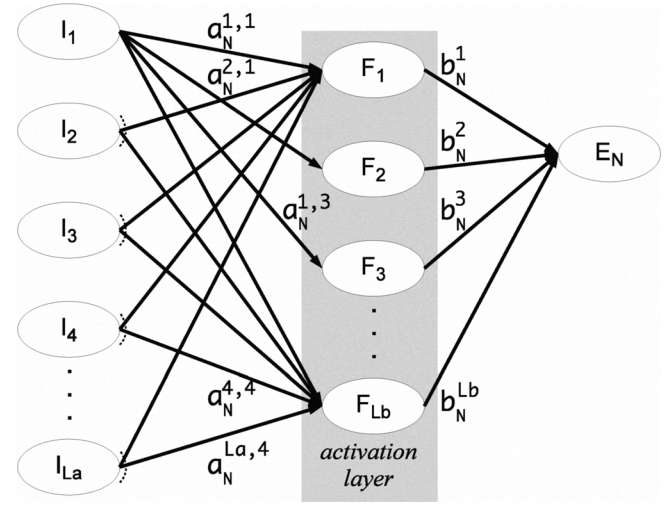


Fig. 1. One of the nine MLP structured networks, showing source nodes on the left handling individual feature vector inputs, the hidden activation layer and output node on the right.

(6): the second matrix in Eqn. (3) can no longer be ignored, and thus the full \mathbf{J} matrix in Eqn. (3) is used in all cases.

After much experimentation, a relatively simple MLP structure, as shown in Fig. 1, was found to be suitable. In this system, L_a input nodes capture a feature vector of CP data, weighting these values and feeding them into the activation layer which consists of a set of L_b nodes which each contain different activation functions. The weighted activation outputs combined yield the reconstructed element E .

The input vector thus consists of the CP data plus a standard MLP bias term:

$$I_n = [j_{11} \ j_{22} \ \Re(j_{12}) \ \Im(j_{12}) \ \beta]. \quad (9)$$

Each of N trained networks, having fixed weights a and b and a predetermined bias, β , generate one of the FP matrix elements using the relationship:

$$E_N = \sum_{i=1}^{L_b} b_i \cdot F_i + \sum_{j=1}^{L_a} a_j \cdot I_j \quad (10)$$

In this system, the use of independent networks for each of the FP output elements leads to faster convergence when training, and results in generally good estimation performance of the individual FP elements, however it does not explicitly constrain possible statistical relations among the output elements.

A. Activation functions

The activation functions for this system are unusual in that they are not equivalent between hidden layer nodes. The full set of functions used within the network are:

$$F = \begin{bmatrix} \delta() \\ \ln() \\ \tanh() \\ \text{logistic}() \end{bmatrix} \quad (11)$$

Obviously, these functions do not contribute equally to the network output result, however each has some particular merit. The use of *sigmoidal* functions (*i.e.* *logistics()*, *tanh()*) is standard in back-propagation neural networks and their significant contribution into the networks' capacity have long been noticed [6]. It is well known that SAR images are inherently affected by multiplicative noise. Evidently, handling multiplicative noise signals in the logarithmic domain transform this to additive noise with Gaussian approximated distribution [7] [8]. The treatment is a tried-and-tested technique for SAR data processing [9]. The intention here is therefore to allow the *ln()* activation function to reduce the sensitivity of the system to multiplicative noise. We explore in Section III whether this is indeed the case. The $\delta()$ provides a direct scaled coupling of the t_{CP} matrix into the result where necessary, particularly useful for the h-h and v-v estimation.

Fig. 1 shows the MLP network design with all synapses having the same learning rate to support batch and stochastic updates. As multiple data sets were taken as training points, batch update was used to ensure error convergence and a standard back-propagation based method used for weight updates. In this system, each single training epoch consisted of an entire set of training areas.

B. Training and test data

Evaluation data was obtained from nine-look NASA/JPL POLSAR C- and L-band images, which cover the area of Muda Merbok, West Malaysia. This area contains a mixture of different land covers, which have been verified through manual ground surveying, and classified into oil palm plantation, rubber plantation, scrub, water and built-up areas. The data thus covers agricultural land use as well as a section of urban area.

The images were manually divided into five equally-sized sections comprising the five land cover classifications above, with each section randomly divided further into training and testing sub-areas. The total image size used for both training and testing was 2540×2831 pixels.

As mentioned in Section II, separate networks were used for the reconstruction of the nine FP matrix elements, and each network was trained independently using the same training data (the networks were also separately trained for L-band and C-band results). One training and back-propagation epoch for each network consisted of one batch-mode training update across all land cover images.

The network cost function D , used for both the training update, and subsequent evaluation, was originally defined as the mean-squared difference, in the logarithmic domain, between the estimated and actual output (*i.e.* the difference between the original FP data element and the corresponding reconstructed FP data element). The use of a logarithmic difference, again, being due to the presence of multiplicative noise. However, it was subsequently found that a combination of linear and logarithmic cost functions was able to slightly

TABLE I
BENCHMARK COMPARISON OF MLP AND LE USING A MEAN SQUARED-ERROR METRIC FOR SEPARATE REGIONS OF C-BAND AND L-BAND RESPECTIVELY

	MLP (mean, sd)	LE (mean, sd)
Built up (recall)	0.07160	0.16950
Built up (validation)	0.08573	0.41658
Oil Palm (recall)	0.00188	0.00294
Oil Palm (validation)	0.00182	0.00375
Rubber (recall)	0.00356	0.00631
Rubber (validation)	0.00472	0.00947
Scrub (recall)	0.00133	0.00227
Scrub (validation)	0.00134	0.00290
Water (recall)	9.58E-6	6.59E-6
Water (validation)	9.39E-6	6.86E-6
Built up (recall)	0.04947	0.19729
Built up (validation)	0.03471	0.18447
Oil Palm (recall)	0.00026	0.00048
Oil Palm (validation)	0.00026	0.00053
Rubber (recall)	0.00258	0.00425
Rubber (validation)	0.00289	0.00554
Scrub (recall)	6.19E-6	1.37E-5
Scrub (validation)	1.82E-5	5.23E-5
Water (recall)	7.05E-6	1.75E-5
Water (validation)	4.67E-6	1.07E-5

TABLE II
BENCHMARK COMPARISON OF MLP AND LE USING A MEAN SQUARED-LOG-ERROR METRIC FOR SEPARATE REGIONS OF C-BAND AND L-BAND RESPECTIVELY

	MLP (mean, sd)	LE (mean, sd)
Built up (recall)	1.24	1.50
Built up (validation)	1.34	1.49
Oil Palm (recall)	0.27	0.46
Oil Palm (validation)	0.28	0.42
Rubber (recall)	0.23	0.28
Rubber (validation)	0.26	0.36
Scrub (recall)	0.25	0.33
Scrub (validation)	0.24	0.40
Water (recall)	1.04	0.76
Water (validation)	1.02	0.74
Built up (recall)	3.02	2.58
Built up (validation)	2.99	2.57
Oil Palm (recall)	0.74	1.17
Oil Palm (validation)	0.72	1.08
Rubber (recall)	0.93	1.07
Rubber (validation)	0.94	1.04
Scrub (recall)	1.27	2.23
Scrub (validation)	1.41	3.06
Water (recall)	4.45	3.47
Water (validation)	3.80	3.30

out-perform the use of the logarithmic function alone:

$$D = \sum_{i=0}^M \frac{\{t_i - o_i\}^2 + \{\ln(t_i) - \ln(o_i)\}^2}{2}. \quad (12)$$

where t and o represent the target and output values of the network over an epoch comprising M distinct training vectors.

Convergence rates were studied, an adaptive update weight applied, and it was found that all networks were able to converge within about 500 training epochs.

III. RESULTS AND DISCUSSION

In this study, the MLP-assisted FP reconstruction was benchmarked against the Linear Extrapolated (LE) approach used by [3] running for ten iterations, across both the training

TABLE III
BENCHMARK COMPARISON OF MLP AND LE USING A MEAN SQUARED-ERROR METRIC FOR SEPARATE REGIONS OF C-BAND AND L-BAND RESPECTIVELY (BUILT-UP TRAINING ONLY)

	MLP (mean, sd)	LE (mean, sd)
Built up (recall)	0.02267	0.12426
Built up (validation)	0.05754	0.48326
Oil Palm (recall)	0.00309	0.00466
Oil Palm (validation)	0.00297	0.00599
Rubber (recall)	0.00959	0.01203
Rubber (validation)	0.01160	0.01573
Scrub (recall)	0.00340	0.00414
Scrub (validation)	0.00344	0.00443
Water (recall)	2.77E-6	2.14E-6
Water (validation)	2.70E-6	2.13E-6
Built up (recall)	0.00348	0.01625
Built up (validation)	0.00189	0.00532
Oil Palm (recall)	0.00049	0.00073
Oil Palm (validation)	0.00048	0.00080
Rubber (recall)	0.00450	0.00582
Rubber (validation)	0.00508	0.00736
Scrub (recall)	3.28E-6	7.25E-6
Scrub (validation)	1.11E-5	2.82E-5
Water (recall)	5.64E-6	3.22E-6
Water (validation)	5.01E-6	2.48E-6

TABLE IV
BENCHMARK COMPARISON OF MLP AND LE USING A MEAN SQUARED-LOG-ERROR METRIC FOR SEPARATE REGIONS OF C-BAND AND L-BAND RESPECTIVELY (BUILT-UP TRAINING ONLY)

	MLP (mean, sd)	LE (mean, sd)
Built up (recall)	0.55	0.77
Built up (validation)	0.58	0.84
Oil Palm (recall)	0.71	0.72
Oil Palm (validation)	0.67	0.74
Rubber (recall)	1.16	0.85
Rubber (validation)	1.23	0.95
Scrub (recall)	1.21	0.90
Scrub (validation)	1.19	0.89
Water (recall)	0.51	0.50
Water (validation)	0.49	0.49
Built up (recall)	0.93	1.06
Built up (validation)	0.97	1.20
Oil Palm (recall)	1.93	1.51
Oil Palm (validation)	1.93	1.50
Rubber (recall)	3.58	2.19
Rubber (validation)	3.55	2.14
Scrub (recall)	0.36	0.57
Scrub (validation)	0.46	0.62
Water (recall)	6.67	2.71
Water (validation)	6.29	2.73

and the test data set, for both L-band and C-band images. Tables I and II present the mean-squared error, and mean-squared log error across each individual element of each pixel for the test and training data sets.

Before examining the data, it is only fair to reiterate that the LE method [3] does not claim to operate well over built-up areas: we present the comparison merely to show the MLP method results over such areas, whilst maintaining similar results to the LE method over other areas.

No major differences in reconstruction performance were observed with respect to the frequency bands, with the trends of both C-band and L-band results being similar. As expected, both CP reconstruction methods operate very well over water,

and both operate poorly over built-up areas. It can be seen that MLP out-performs LE slightly in all areas apart from water, and more significantly over built-up areas, especially considering the mean squared error results.

The important h-v component of the reconstructed matrices is presented in Fig. 2, where original and reconstructed image sections of built up and oil palm areas, using both methods, are reproduced. The figure also plots the histograms of the image intensities, showing that the shape of the MLP-reconstructed intensity histogram is more faithful to the original than is the LE-reconstructed intensity histogram. Finally, difference plots, which indicate the linear intensity difference between the original images and the reconstructed images (where black indicates the images are identical, and white indicates a significant difference), reveal that both methods fail to match the original exactly for both area types.

In order to explore the reconstruction performance over built up areas, the MLP systems were re-trained using *only* built-up image areas, and the evaluation repeated. The results, shown in Tables III and IV reveal a significant improvement in the performance of the MLP system over built up areas, at the cost of a performance reduction in several other areas.

At this point, it is clear that the results are promising, however it must be noted that the work described in this study also has its own short-comings. Firstly, the cross-FP element relationships are still left un-exploited, due to the use of independent networks to train each element. Secondly, the particular network topology used is computationally more intensive than the linear-extrapolation approach of Souyris et al.

IV. CONCLUSION

This paper has presented a novel approach to the reconstruction of FP data from a CP representation, with the focus on the compact polarimetry $\pi/4$ mode, using a MLP-based neural network. The major advantage of the approach described is that it operates without making any symmetry assumption.

The system was trained using multi-look NASA/JPL POLSAR images in both C- and L-band, and evaluated by comparison with an existing pioneering method for various land cover types. In particular, one of the land areas used, that of a built up area, does not comply with the symmetry assumption.

Results, expressed as the mean-squared difference, and mean-squared logarithmic difference between source FP data and output FP data (reconstructed by each method from CP images derived through an exact transformation of the source FP data), indicate that the MLP-based system performs reasonably well for all tested land cover types, and in particular shows promise for the reconstruction of FP data over built up areas. When the h-v intensity image is plotted in Section III, the abilities of the MLP system can be visualised, both for the built up areas, and also for one type of agricultural area.

REFERENCES

- [1] D. Massonnet and J. Souyris, *Imaging with Synthetic Aperture Radar*. CRC Press, 2008.

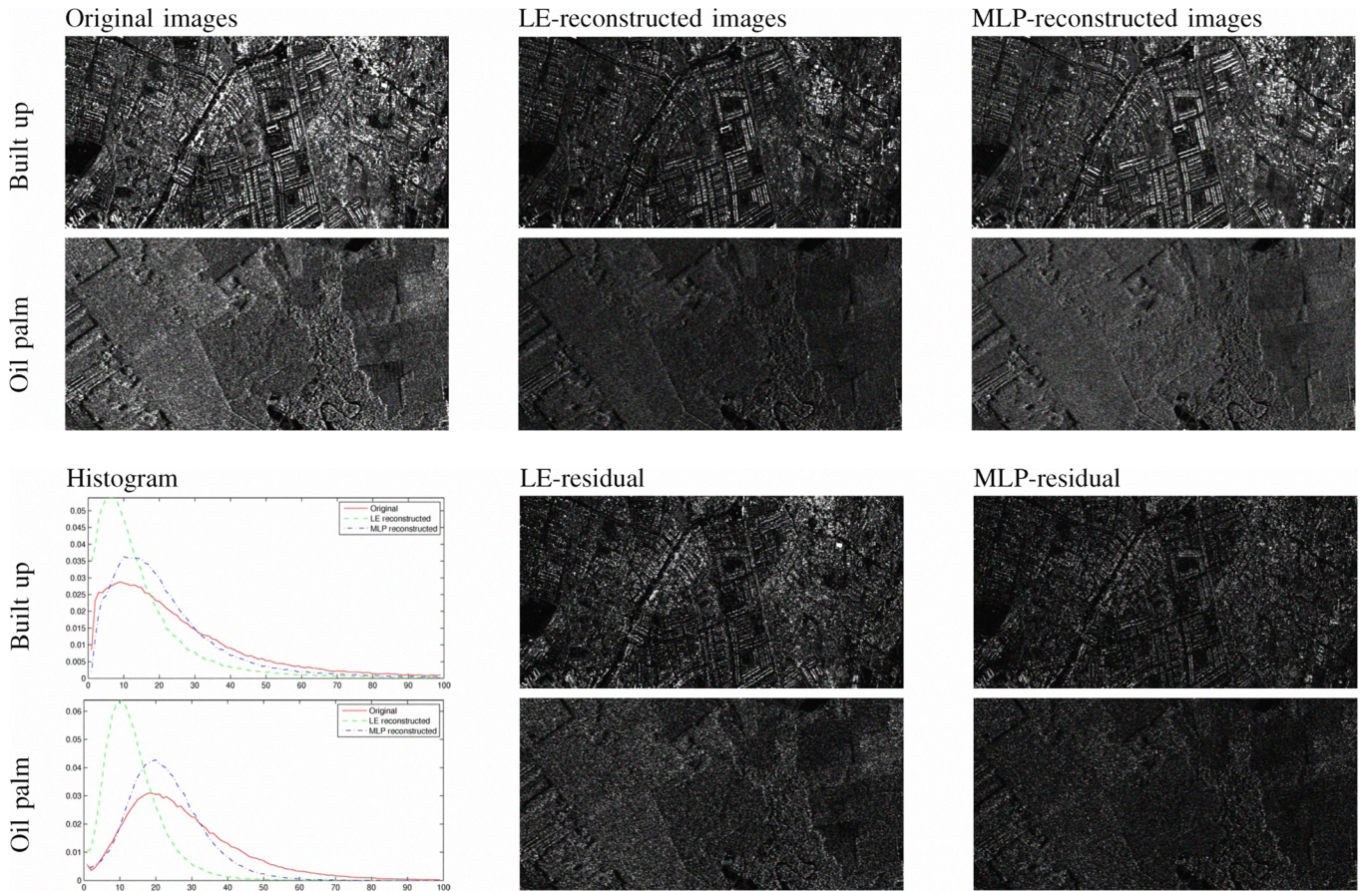


Fig. 2. h-v intensity plots of the original, LE-reconstructed and MLP-reconstructed images for an oil palm area and a built up area (top and second row from the top, respectively). Below this are the image intensity histograms after applying an absolute saturation threshold of 0.5 (so that image intensities greater than 0.5 are saturated), with an x-axis ranging from 0 to 100% saturation. The remaining subplots on the bottom two rows show the linear difference between the original and reconstructed images as plotted above, without applying any further intensity scaling, so that black indicates areas where the reconstructed and original h-v pixel magnitudes are identical, and where white indicates significant differences. A perfect reconstruction would thus have a completely black difference image, and an ideal reconstruction would contain no discernable information.

- [2] H. Zebker and J. V. Zyl, "Imaging radar polarimetry: A review," *Proc. IEEE*, vol. 79, no. 11, pp. 1583–1606, Nov. 1991.
- [3] J. Souyris, P. Imbo, R. Fjortoft, S. Mingot, and J. Lee, "Compact polarimetry based on symmetry properties of geophysical media," *IEEE Trans. Geosci. Remote Sens.*, vol. 43, no. 3, pp. 634–646, Mar. 2005.
- [4] S. Nghiêm, S. Yueh, R. Kwok, and F. Li, "Symmetry properties in polarimetric remote sensing," *Radio Sci.*, vol. 27, no. 5, pp. 693–711, Oct. 1992.
- [5] M. Nord, T. Ainsworth, J. Lee, and J. Stacy, "Comparison of compact polarimetric synthetic aperture radar mode," *IEEE Trans. Geosci. Remote Sens.*, vol. 47, no. 1, pp. 634–646, Jan. 2009.
- [6] R. Nielsen, "Theory of the backpropagation neural network," *Neural Network for perception (Vol 2): computation, learning, architecture*, vol. 2, no. 4, pp. 303–314, Feb. 1989.
- [7] H. Arsenault and G. April, "Properties of speckle integrated with a finite aperture and logarithmically transformed," *J. Opt. Soc. Am.*, vol. 66, no. 11, pp. 1160–1163, Nov. 1976.
- [8] H. Xie, L. Pierce, and F. Ulaby, "Statistical properties of logarithmically transformed speckle," *IEEE Trans. Geosci. Remote Sens.*, vol. 40, no. 3, pp. 721–727, Mar. 2002.
- [9] A. Achim, P. Tsakalidesz, and A. Bezerianosy, "SAR image denoising via Bayesian wavelet shrinkage based on heavy-tailed modeling," *IEEE Trans. Geosci. Remote Sens.*, vol. 41, no. 8, pp. 1773– 1784, Aug. 2003.